van der Waals-like transition in fluidized granular matter: hydrodynamic description

R. Soto, M. Argentina, and M.G. Clerc

Departamento de Física, Facultad de Ciencias Físicas y Matemáticas, Universidad de Chile, Casilla 487-3, Santiago, Chile.

Abstract

A phase separation of fluidized granular matter is presented. Molecular dynamics simulations of grain system, in two spatial dimensions, with a vibrating wall and without gravity exhibit appearance, coagulation, and evaporation of bubbles. The instability is produced by the existence of a negative compresibility region, that is caused by the energy dissipation at collisions. The phenomenon is analogous to the spinodal decomposition of the gas-liquid transition of the van der Waals model. A hydrodynamic model gives account for the negative compresibility and predicts a critical point that is in qualitative agreement with the results of the simulations. In the onset of phase separation, we have deduced a macroscopic model that agrees quite well with molecular dynamics simulations.

Key words: Granular fluid, spinodal decomposition, instability
PACS: 45.70.-n, 05.45.-a, 64.75.+g

Granular matter, when fluidized by continuous energy injection exhibits a variety of phenomena that resembles those of molecular fluids: patterns and instabilities appear, Rayleigh-Benard like convection is developed, etc [1–3]. The main difference with molecular fluids is that, at collisions, grains dissipate kinetic energy into the internal degrees of freedom of the grains. Hence energy must be supplied continuously to sustain a fluidized regime. Experimentally, energy is usually injected through vibrating walls or by the gravitational field.

Fluidized granular systems have the tendency to create large gradients in the hydrodynamic fields, and microscopic and macroscopic time and length scales are not enough separated as in elastic fluids [4]. However, when dissipation is not too large, fluidized regimes of granular matter are described successfully using hydrodynamic models. These models are similar to the Navier-Stokes equations for elastic fluids, with the addition of an energy dissipation term.

Email address: rsoto@dfi.uchile.cl (R. Soto) .

Here, we describe a new type of instability observed in fluidized granular matter (reported previously in Ref. [5]), analogous to the spinodal decomposition of the gas-liquid transition in the van der Waals model [6]. The origin of the instability relies on the fact that for granular media the average granular temperature is a decreasing function of the density for fixed boundary conditions. This results in negative compressibility for dissipation larger than a critical value giving rise to a spatial instability. We also show that the instability can be understood using a simple hydrodynamic model.

We consider a two-dimensional system of grains on an horizontal surface, with friction ignored, placed in a box with large aspect ratio (see Fig. 1). Henceforth, we will refer to horizontal and vertical directions as the long and short directions, respectively; the system is periodic in the horizontal direction. The top wall reflects grains elastically while the bottom one injects energy into the system by means of a vibrating wall at high frequency ω and small amplitude A. The collisions with the wall are elastic with no friction, thus conserving horizontal momentum. Due to the high frequency, the collisions with the wall are uncorrelated, being modeled in a stochastic way. For simplicity, the vibrating wall is well modeled by a stochastic wall: each time a grain collides with the wall, it is reflected conserving the tangential component of the velocity, but the normal component is sorted from a Maxwellian distribution at a certain temperature, that scales as $T \sim m(A\omega)^2$, m being the mass of the gains [7]. We define the granular temperature (the *temperature* from now on), like in molecular fluids, to be proportional to the kinetic energy per particle in the reference frame of the fluid. We emphasize that both collisions with the walls and between the grains conserve horizontal momentum.

The system is studied using molecular dynamics simulations of the Inelastic Hard Sphere model (IHS) [8–10]. Grains are modeled as smooth rigid disks and the collisions are characterized by a constant normal restitution coefficient α. Grains only have translational degrees of freedom and there is no tangential friction between grains at collisions. The IHS has been widely studied and reproduces well many of the observed phenomena in granular fluids at moderate densities, where rotation is not fundamental (see, for example, [8–10]). Units are chosen such that the diam-

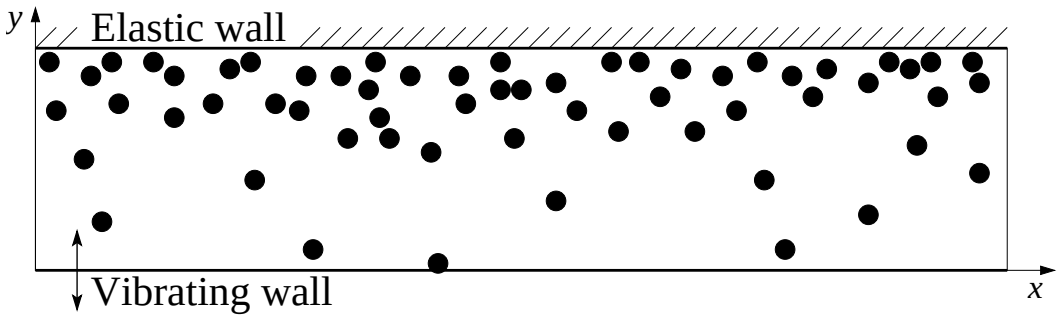

Fig. 1. Schematic representation of the studied system. Grains are placed in an horizontal box. The bottom wall is vibrating while the top one reflects grains elastically. The system is periodic in the x direction.

eter σ and mass m of each disk is one. Also, taking the wall temperature as one, energy units are fixed. Under these conditions, the system is completely defined by the total number of grains N, the aspect ratio $\lambda = L_x/L_y \gg 1$, the global number density $n_0 = N/(L_x L_y)$, and the restitution coefficient of the grains $\alpha = (1-2q)$; the elastic limit corresponds to $q = 0$.

At low dissipation, the granular media develops vertical density and temperature profiles induced by the dissipation at collisions and the energy injection mechanism, but both fields are homogeneous in the horizontal direction. The system is hotter and less dense near the injecting wall, and colder and denser by the opposite wall (see Fig. 1).

For a larger dissipation ($N = 153600$, $\lambda = 102.4$, $n_0 = 0.15$, $L_x = 10240$, and $q = 0.02$) an spatial instability is observed: the system exhibits the coexistence of two fluid phases, characterized by different densities (see Fig. 2). Initially the fluid remains horizontally homogeneous and suddenly a bubble (low density region) appears and grows until it achieves its final size. After that, the system remains stationary with the two phases coexisting.

To characterize in more detail this instability, we analyze the temporal evolution of the vertically averaged density (*coarse grained density*) $\rho(x,t) = L_y^{-1} \int_0^{L_y} n(x,y,t)dy$, where $n(x,y,t)$ is the density field. In Fig. 3 the spatio-temporal evolution of $\rho(x,t)$ is presented. It is clearly seen that the system remains in a homogeneous state for a finite large time until the bubble is nucleated due to density fluctuations. Therefore, this homogeneous state is a metastable one. Afterwards, the bubble grows with a nearly constant velocity while two densification fronts propagate away from the bubble at a larger, but also constant, velocity (illustrated in Fig. 3). When the fronts reach the growing bubble —through the periodic boundary conditions— it

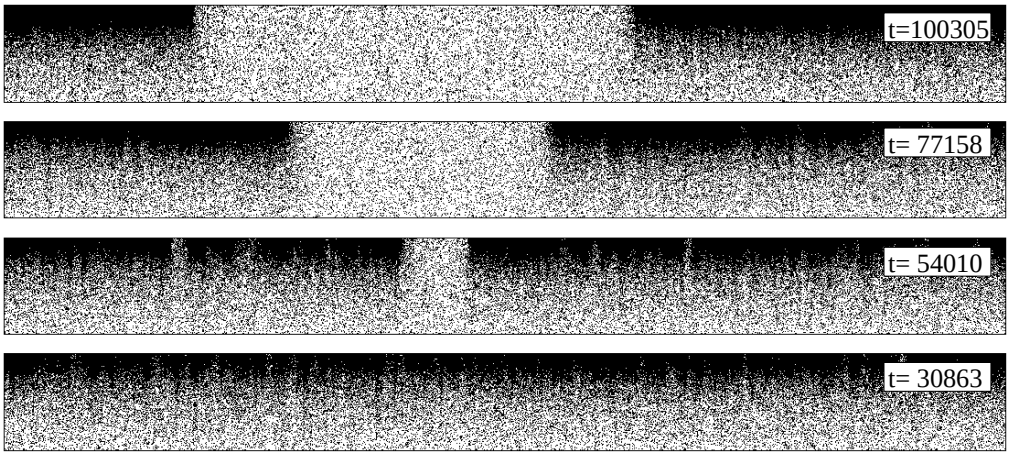

Fig. 2. Snapshots of a system with $N = 153600$, $\lambda = 102.4$, $n_0 = 0.15$, $L_x = 10240$, and $q = 0.02$. The configurations correspond to different simulation times. Each black dot represents a simulated grain and the aspect ratio has been distorted to make the system visible. The bubble appears at $t \approx 40000$.

is pushed inwards, leading to damped oscillations in its size. Finally, the system achieves a stationary state with the bubble.

The system shows a different behavior, according to the value of the dissipation parameter q. In Fig. 4 the spatiotemporal evolution of a system with a smaller dissipation is shown ($q = 0.01$). In this case four bubbles are created in the fluid with no apparent metastable time. Two of them merge into a single one, and later on, the smallest one disappears or evaporates. Later on the two remaining bubbles evolve

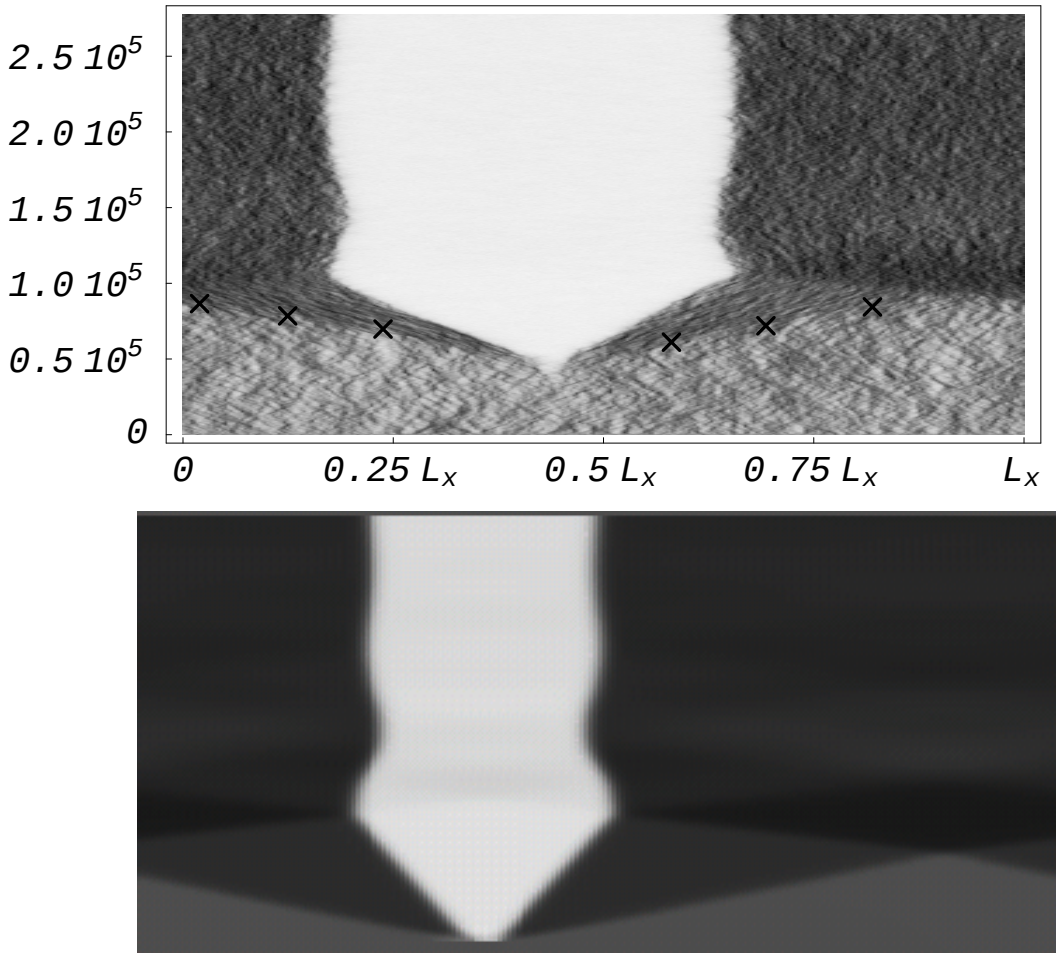

Fig. 3. Spatiotemporal evolution of the coarse grained density $\rho(x,t)$, with time on the vertical axis and increasing upwards. The gray scale is proportional to density, with darker regions representing denser regions in the system. The top graph corresponds to the molecular dynamics simulation with the same parameters as in Fig. 2, where the bubble nucleation is triggered by internal noise. In the final state, the vertically averaged density of the bubble is $\rho = 0.025$, while in the dense region $\rho = 0.257$. The densification fronts are marked with lines of crosses. The bottom graph is obtained by the simulation of the model defined by Eq. (11) with $\varepsilon = -6.6 \times 10^{-4}$ and $v = 2$. The system size is 5400 and the total simulation is time $T = 3.5 \times 10^5$. An initial condition (with $u = 1.4 \times 10^{-2}$) that overcomes the nucleation barrier is imposed. The minimum (light gray) and maximum (dark gray) densities are $u = -2.6 \times 10^{-2}$ and $u = 2.9 \times 10^{-2}$, respectively.

slowly, one of them growing while the other one decreases. Densification fronts, created with the bubbles, are also seen.

We have also made a series of simulations keeping constant the value of q and changing the value of the global density n_0. All the simulations were done with the following parameters $N = 153600$, $q = 0.02$, and $L_y = 100$. The spatio-temporal evolution of the coarse grained density $\rho(x,t)$ is represented in Fig. 5 for different values of n_0. For global densities smaller that $n_0 = 0.03$ the system remains stable; for densities between $n_0 = 0.033$ and $n_0 = 0.15$ the system is unstable or metastable and depending on the case low density regions (bubbles) or large density ones (droplets) are created; finally for densities larger than $n_0 = 0.25$ no instabilities were observed. Note that in all cases (specially visible for $n_0 = 0.03$) density waves created by density fluctuations are observed in the background re-

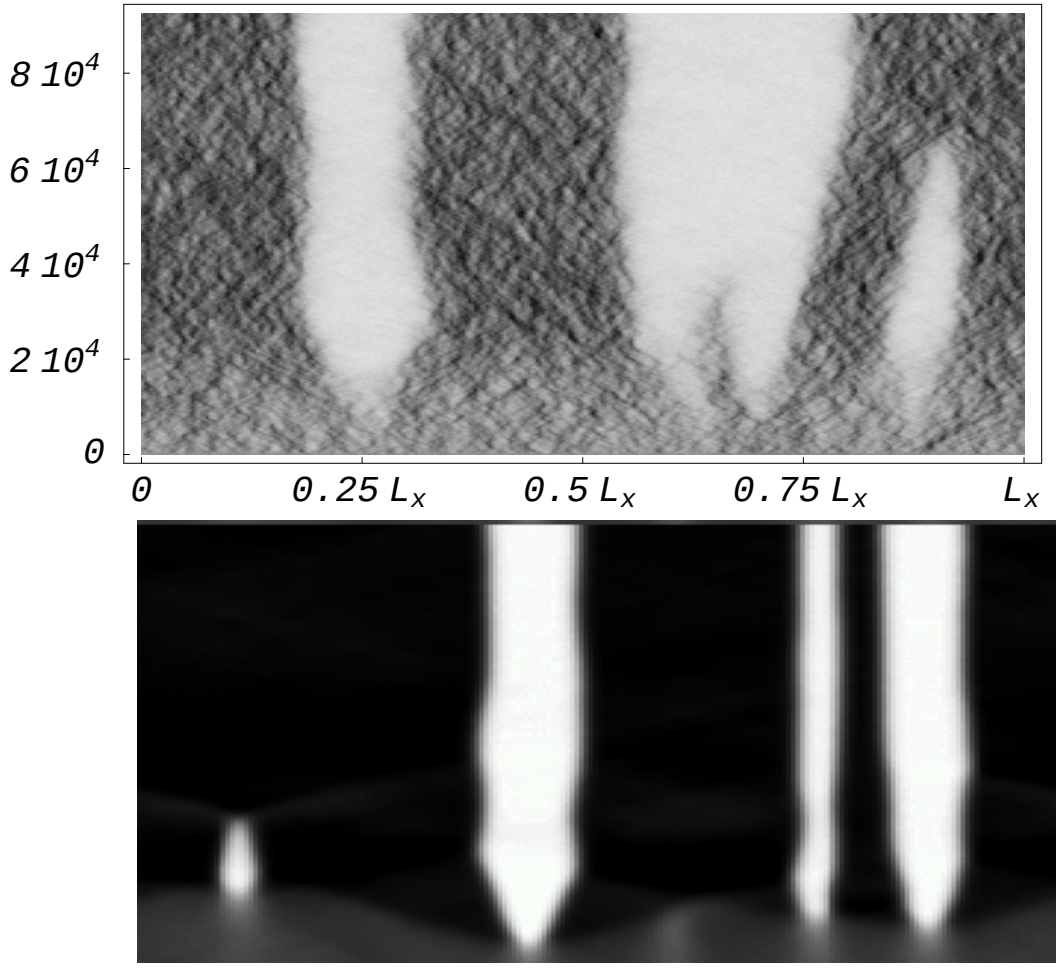

Fig. 4. The same representation as in Fig. 3, but changing the dissipation parameter to $q = 0.01$. In the final simulated state, the vertically averaged density of the bubbles is $\rho = 0.046$, while in the dense regions $\rho = 0.216$. In the bottom graph, we use the same parameters and gray scale as in Fig. 3 and the initial condition is $u = 7.4 \times 10^{-3}$. In this case there is no nucleation barrier and the initial condition used in the solution of the model is homogeneous with small fluctuations that are amplified by the instability.

gions. These waves propagate with well defined velocities.

The observed behavior is similar to the van der Waals gas liquid transition, where for temperatures lower that the critical one, there is a density range for which the homogeneous state is unstable. Here, in the granular fluid, the control parameter is the dissipation coefficient q instead of the thermodynamic temperature.

The origin of the instability can be understood as follows. In thermodynamic equilibrium, the pressure is a monotonous increasing function of the density and the temperature [11]. But, in this system, the granular temperature adjusts itself to a stationary profile given by the energy balance between dissipation at collisions and injection at the vibrating wall. As the dissipation rate is proportional to density, the stationary temperature is a decreasing function of ρ. As an outcome, the effective pressure (that is independent of y due to the absence of gravity) can present a region where it decreases with an increasing density. That is, the temperature drop produced by collisions can be large enough to give rise to a decrease in pressure when increasing the global density [12]. Then, there can be a region of negative compresibility in the same sense as the van der Waals loop in classical fluids, that triggers the instability.

The existence of the negative compresibility region can be verified numerically as follows. We have performed molecular dynamics simulations of the IHS system in tall boxes ($L_x \ll L_y$) to prevent the spatial instability to develop: when the horizontal system size is small, there is a large surface energy cost in creating a bubble, and the system remains stable. We compute the horizontal momentum flux (x–x component of the pressure tensor, p_{xx}), averaged over the vertical direction for different values of the global density n_0 and the dissipation coefficient q.

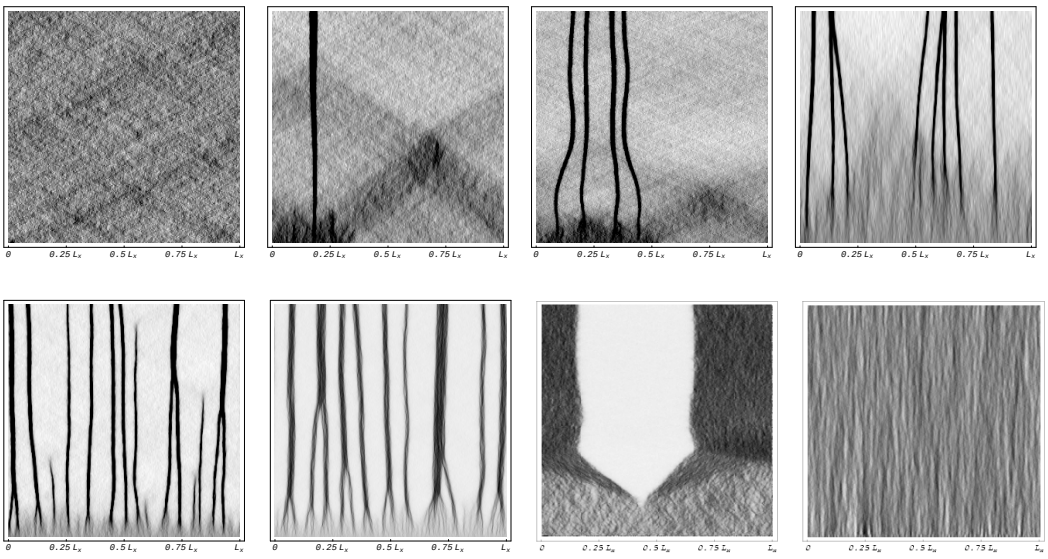

Fig. 5. Spatiotemporal evolution of the coarse grained density $\rho(x,t)$. All the simulations are done with $N = 153600$, $q = 0.02$, and $L_y = 100$. The simulations differ in the global density; from left to right and top to bottom the densities are $n_0 = 0.03, 0.033, 0.035, 0.04, 0.05, 0.08, 0.15$, and 0.30.

For constant q, the pressure p_{xx} exhibits the appearance of van der Waals loops, with a critical point located at $q \approx 0.0047$ and $\rho \approx 0.15$ (see Fig. 6). For larger values of q there is a region with negative compresibility ($\partial p_{xx}/\partial n_0 < 0$) that is bounded by the spinodal curve. Also, we can compute the coexistence curve using Maxwell's construction. The region between the coexistence and spinodal curves define the bistability region, where bubbles or droplets can nucleate thanks to density fluctuations. Inside the spinodal curve, the system is mechanically unstable. We remark that the Maxwell construction for computing the coexistence curve if valid for thermodynamic equilibrium systems; however, as it will be shown later, close to the instability critical point the system dynamics is governed by a free energy (Landau type) and the Maxwell construction can be done.

The existence of the negative compresibility region can be studied theoretically using a hydrodynamic description of granular fluids. We consider the simplest hydrodynamic equations that mimic the Navier-Stokes ones with a dissipation term in the energy equation, modeling the energy dissipation at collisions. For sufficiently small dissipation ($q \ll 1$), one has [13–16]

$$
\begin{aligned}
&\frac{\partial n}{\partial t} + \nabla \cdot (n\mathbf{v}) = 0, \\
&n\left(\frac{\partial \mathbf{v}}{\partial t} + (\mathbf{v}\cdot\nabla)\mathbf{v}\right) = -\nabla \cdot \mathbb{P}, \\
&n\left(\frac{\partial T}{\partial t} + (\mathbf{v}\cdot\nabla)T\right) = -\nabla\cdot\mathbf{J} - \mathbb{P} : \nabla\mathbf{v} - \omega,
\end{aligned}
\tag{1}
$$

with the usual constitutive equations for the pressure tensor (hydrostatic pressure and Newton's law) and the Fourier's law for the heat, and the new constitutive equation for the energy dissipation rate flux,

$$
\begin{aligned}
\mathbb{P}_{i,j} &= p(n,T)\delta_{i,j} - \eta(n,T)\left(\frac{\partial v_i}{\partial x_j} + \frac{\partial v_j}{\partial x_i}\right) - (\xi(n,T) - \eta(n,T))\nabla\cdot\mathbf{v}\delta_{i,j} \qquad (2)\\
\mathbf{J} &= -k(n,T)\nabla T \\
\omega &= \omega_0(n,T)n^2T^{3/2}.
\end{aligned}
$$

The transport coefficients in the limit of small dissipation are the same as for elastic spheres in 2D [17], except for the one associated to the energy dissipation, that is calculated directly using the Enskog theory [18]. All the transport coefficients are expressed in terms of the pair correlation function of elastic disks at contact, χ.

$$\chi(n) = \frac{1-7\pi n/64}{(1-\pi n/4)^2} \tag{3}$$

$$p(n,T) = nT\frac{\left(1+\pi^2 n^2/128\right)}{(1-\pi n/4)^2} \tag{4}$$

$$\eta(n,T) = \frac{1}{2\chi}\left(1+\pi n\chi/2+0.87(\pi n\chi/2)^2\right)\sqrt{\frac{T}{\pi}} \tag{5}$$

$$\xi(n,T) = \frac{1.246}{2\chi}(\pi n\chi/2)^2\sqrt{\frac{T}{\pi}} \tag{6}$$

$$k(n,T) = \frac{2}{\chi}\left(1+3\pi n\chi/4+0.87(\pi n\chi/2)^2\right)\sqrt{\frac{T}{\pi}} \tag{7}$$

$$\omega_0 = 4\sqrt{\pi}q\chi(n) \tag{8}$$

In the model (1), density and horizontal momentum satisfy conservation equations. We consider that the the velocity field is small enough to neglect nonlinear terms in **v**. Density and horizontal momentum can be vertically averaged giving $\rho(x,t)$ and $j(x,t)$, that obey the equations

$$\partial_t \rho\,(x,t) = -\partial_x j\,(x,t)\,, \tag{9a}$$

$$\partial_t j\,(x,t) = -\partial_x \Phi, \tag{9b}$$

where Φ is the vertical average of the $x-x$ component of the pressure tensor.

When the horizontal gradients are small compared to the vertical ones, ρ and j behave as slow variables and govern the system dynamics. The other fields (vertical momentum, temperature, and Φ) have fast dynamics and behave as slave variables of ρ and j.

The value of Φ can be computed using the equations for the temperature and vertical momentum. The vertical momentum relaxes fast to its equilibrium value, zero, due to the boundary conditions. Then, the pressure is independent of y ($\Phi = p$). Energy is not conserved implying that temperature is also a fast variable and satisfies the equation $\nabla\cdot\mathbf{J}+\omega = 0$. The equations of T and Φ can be solved numerically with the boundary conditions $T = 1$ at the bottom and $\mathbf{J} = 0$ at the top, and the integral condition $\int_0^{L_y} n(x,y,t)dy = L_y\rho(x,t)$.

For fixed q, the pressure exhibits, as proposed before, van der Waals loops as a function of $n_0 = \rho(x,t)$ (see Fig. 6). The negative compresibility region has a critical point at $q \approx 0.0086$ and $n_0 \approx 0.11$. This is in qualitative agreement with the molecular dynamics simulations in tall boxes. The difference is originated mainly in the boundary condition for T. Indeed, even though particles are forced to come out of the bottom wall with velocities characteristic of a temperature equal to 1, the granular temperature at the boundary is less than one because, due to dissipation, the particles that arrive at the wall come with a smaller kinetic energy. This is a well known effect in dilute gases (Knudsen layer effects [19]), that become also

important in granular fluids.

Having verified that the mechanism that originates the instability is a negative compressibility in the effective pressure, we can describe the dynamics of the dominant mode near the bifurcation point (critical point in the van der Waals language). The critical point is defined by the condition that both $\partial\Phi/\partial\rho$ and $\partial^2\Phi/\partial\rho^2$ vanish. Using symmetry and scaling arguments it can be argued that the averaged pressure Φ close to the critical point can be written as (see Ref. [5])

$$\begin{aligned}\Phi \approx \Phi_o + \frac{\partial\Phi}{\partial\rho}\bar{\rho} + \frac{\partial^2\Phi}{\partial^2\rho}\frac{\rho^2}{2} + \frac{\partial^3\Phi}{\partial^3\rho}\frac{\rho^3}{6} + \frac{\partial\Phi}{\partial j^2}j^2 \\ + \frac{\partial\Phi}{\partial\rho_{xx}}\rho_{xx} + \frac{\partial\Phi}{\partial j_x}j_x,\end{aligned} \tag{10}$$

For sake of simplicity, we define now $u = \rho - \rho_M$, where ρ_M is the density at the Maxwell point (i.e. where $\partial^2\Phi/\partial^2\rho\big|_{\rho_M} = 0$). Scaling u and x, Eqs. (9) are approximated at the dominant order by the *Van der Waals normal form*

$$\begin{aligned}\partial_{tt}u &= \partial_{xx}\left(\varepsilon u + u^3 - \partial_{xx}u + \nu\partial_t u\right), \\ &= \partial_{xx}\frac{\delta\mathscr{F}}{\delta u} + \nu\partial_{xxt}u,\end{aligned} \tag{11}$$

where $\varepsilon = \partial\Phi/\partial\rho|_{\rho_M}$ is the control parameter and $\nu\partial_{xxt}u$ is a diffusion term. The variables scale as $u \sim \varepsilon^{1/2}$, $j \sim \varepsilon$, $\partial_x \sim \varepsilon^{1/2}$, $\partial_t \sim \varepsilon$ and $\nu \sim o(1)$. Note that, the convection term in the momentum flux ($\frac{\partial\Phi}{\partial j^2}j^2 \sim \varepsilon^2$) has been neglected, in comparison with the dominant part (order $\varepsilon^{3/2}$). The sign of $\partial\Phi/\partial\rho_{xx}|_{\rho_M}$ has been chosen to be negative, in order to saturate the linear instability and to impose the existence of a global minimum for the free energy $\mathscr{F} = \int dx\left\{\varepsilon\frac{u^2}{2} + \frac{u^4}{4} + \frac{(\partial_x u)^2}{2}\right\}$.

We emphasize that the Landau free energy $\mathscr{F}$ has the classical phase diagram, with coexistence and spinodal curves [20]; as those observed in binary fluids, binary alloys, and $^3He-^4He$ mixtures, to mention a few examples (see [6] and references cited therein).

For negative ε, the homogeneous solution ($u = 0$) undergoes a spatial instability, characterized by the appearance of equally distributed bubbles. Later on, closest bubbles merge into a bigger one, as a consequence of a coalescence process. Subsequently, bubble dynamics is led by the interaction mediated by waves (see Figs. 4 and 5). The above dynamics is a consequence of the system tendency to minimize its free energy. With periodic boundary conditions, the global minimum is a unique bubble, as the solution shown in Fig. 3. Further work in this coarsening process is in progress.

In the bistability region (see Fig. 6), i.e. the region bounded by the spinodal and coexistence curves, the homogeneous state is stable. Nevertheless, a finite fluctu-

ation that overcomes the nucleation barrier gives rise to a bubble along with two *state-waves (densification waves)*, which propagate away from the bubble as a result of mass conservation (see Fig. 3) . Due to the periodic boundary conditions, later on, the waves collide with the bubble producing its oscillation. Afterwards, due to viscosity, the oscillations are damped and the final state is a single bubble at rest.

The numerical solutions of Eq. (11) (see Figs. 3 and 4) in the unstable and bistable regions show good qualitative agreement with the molecular dynamic simulations. That is, the model captures the main features of the system dynamics close to the instability (density waves, fronts, metastability, and instability).

The model (11) implies that for global densities smaller than the Maxwell point density ($u < 0$), dense regions (instead of low density regions) can nucleate. This prediction is in agreement with the simulations presented in Fig. 5, where one of many dense regions are nucleated for $n_0 < 0.05$. The dynamics of $\rho(x,t)$ is, however, not completely well described by the model because these simulations are done with parameters not close to the critical point. The case of $n_0 = 0.03$ is special, because in this case a long wavelength density modulation is created before the droplet appears. This phenomenon is not captured by the model.

In summary, we have studied the phase separation in fluidized granular matter.

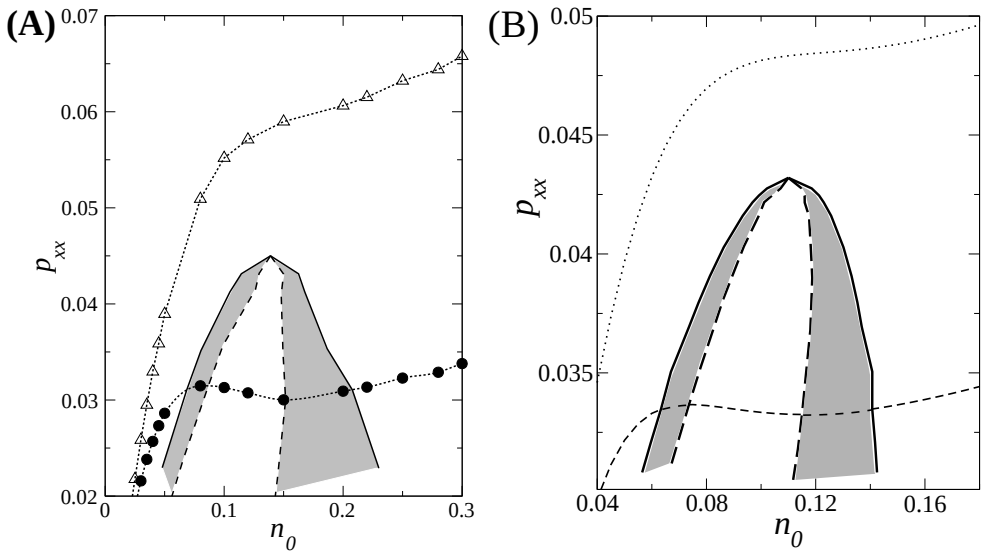

Fig. 6. **(A)** Phase diagram obtained from molecular dynamics simulations in tall, narrow boxes. The dotted curves correspond to the horizontal component of the pressure tensor p_{xx} for the dissipations $q = 0.0032$ (open triangles) and $q = 0.0070$ (filled circles), smaller and larger than the critical one, respectively. The second case presents a van der Waals loop. The coexistence curve (solid line) and spinodal curve (dashed line) are plotted. **(B)** Phase diagram obtained from the hydrodynamic normal form. The solid line (long-dashed) curve is the coexistence (spinodal) curve. The gray region is the bistability region. The dotted (short-dashed) curve correspond to the hydrodynamic pressure for the dissipation $q = 0.007$ ($q = 0.0130$).

Molecular dynamics simulations of a grain system, in two dimension, with a vibrating wall and no gravity exhibit appearance, coagulation and disappearance of low density regions (bubbles). Rarefaction and densification density waves lead the bubble dynamics. The mechanism of phase separation is triggered by a negative compressibility which, in turns, is a result of the fact that for granular media in closed geometries the granular temperature is a decreasing function of the density.

A simple hydrodynamic model is able to predict the existence of van der Waals loops in the effective pressure. The predicted critical point is in qualitative agreement with the results of molecular dynamic simulations.

Close to the transition, the system is described by the van der Waals normal form (11). This model describes quite well the molecular dynamics simulations. The phase separation is the analog to the spinodal decomposition of the gas-liquid transition of the van der Waals model, but the transient evolution of the system is led by state-waves.

The van der Waals instability should be observed independently of the peculiarities of the energy injection mechanism or of its stochastic modelization, as long as the particle collisions with the wall conserve horizontal momentum. It should also be observed in the presence of a small gravitational field either by inclining slightly the table or by placing the system vertically with characteristic injected energy much larger than the gravitational potential energy ($m(A\omega)^2 \gg mgL_y$). In both possible generalizations, the general theoretical framework continues to be valid, and preliminary numerical simulations confirm it (in preparation).

The authors would like to thank P. Cordero, D Risso, and E. Tirapegui for fruitful discussions. The simulation software developed at INLN, France, has been used for the simulations of model (11). M.G.C. and R.S. thank the support of *Programa de inserción de científicos chilenos* of Fundación Andes. M.A. and R.S. greatly thank the support of the FONDECYT projects 30000017 and 1010416, respectively. FONDAP.

References

[1] P. B. Umbanhowar, F. Melo, and H. L. Swinney, Nature **382**, 793 (1996).

[2] R. Ramírez, D. Risso, and P. Cordero, Phys. Rev. Lett. **85**, 1230 (2000).

[3] Y. Forterre and O. Pouliquen, Phys. Rev. Lett. **86**, 5886 (2001).

[4] M-L. Tan and I. Goldhirsch, Phys. Rev. Lett. **81**, 3022 (1998); L. Kadanoff, Rev. Mod. Phys. **71**, 435 (1999). B.J. Glasser and I. Goldhirsch, Phys. Fluids **13**, 407 (2001).

[5] M. Argentina, M. Clerc, and R. Soto, Phys. Rev. Lett. (2002 to appear).

[6] J. D. Gunton, M. San Miguel, and P. S. Sanhi, in *Phase transitions and critical phenomena, volume 8*, edited by D. Domb and J. L. Lebowitz (Academic Press, London, 1983), pp. 267–466.

[7] S. Warr and J. M. Huntley, Phys. Rev. E **52**, 5596 (1995).

[8] I. Goldhirsch and G. Zanetti, Phys. Rev. Lett. **70**, 1619 (1993).

[9] P. Zamankhan, A. Mazouchi, and P. Sarkomaa, Appl. Phys. Lett. **71**, 3790 (1997).

[10] D. C. Rapaport, Physica A **249**, 232 (1998).

[11] L. D. Landau and E. M. Lifshitz, *Statistical physics* (Pergamon Press, New York, 1969).

[12] This mechanism is similar to the one giving rise to the clustering phenomena [8]. Nevertheless, is this later case the granular temperature is not an slave variable.

[13] J. T. Jenkins and M. W. Richman, Arch. Rat. Mech. **87**, 355 (1985).

[14] J. J. Brey, F. Moreno, and J. W. Dufty, Phys. Rev. E **54**, 445 (1996).

[15] C. Bizon, M. D. Shattuck, J. B. Swift, and H. L. Swinney, Phys. Rev. E **60**, 4340 (1999).

[16] R. Soto, M. Mareschal, and D. Risso, Phys. Rev. Lett. **83**, 5003 (1999).

[17] D. Gass, J. Chem. Phys **54**, 1898 (1971).

[18] S. Chapman and T. G. Cowling, *The Mathematical Theory of Non-Uniform Gases*, 3rd ed. (Cambridge University Press, New York, 1970).

[19] C. Cercignani, *Theory and application of the Boltzmann equation* (Elsevier, Amsterdam, 1975).

[20] J. W. Cahn and J. E. Hilliard, J. Chem. Phys. **28**, 258 (1958).